URSI GASS 2020, Rome, Italy, 29 August - 5 September 2020

Mutual Validation of a Fast Solver Based on the Multilevel Nonuniform Grid Approach and an Asymptotic Approximation for High-Frequency Scattering by Strongly Elongated Spheroids

Evgeny V. Chernokozhin*(1), Ivan V. Andronov(2), and Amir Boag(1)
(1) Tel Aviv University, Tel Aviv 69978, Israel
(2) St. Petersburg State University, Russia

Abstract

A fast solver based on the multilevel nonuniform grid approach and an asymptotic approximation designed for scattering by strongly elongated spheroids are mutually validated. Good agreement between the numerical and asymptotic solutions is observed over a wide frequency range for spheroids with various aspect ratios. Numerical noise of the numerical solution is estimated.

1 Introduction

The recently developed "fast" methods for calculating wave scattering, such as the multilevel fast-multipole algorithm (MLFMA) [1] and the multilevel nonuniform grid (MLNG) approach [2], can significantly extend the range of rigorous numerical simulation, far beyond the range of the "conventional" numerically rigorous methods such as the Boundary Element Method (BEM). Based on the traditional approximation of the integral equations, the MLFMA and MLNG algorithm are significantly faster and less memory consuming than the conventional BEM. This enables one to use the fast methods in the range of frequencies and scatterer sizes traditionally considered to be in the range of high-frequency asymptotic methods, e.g., physical optics.

The validation of the fast methods in the high-frequency region is hampered by the lack of exact solutions. A good opportunity for nontrivial validation is provided by the comparison to various asymptotic solutions. For asymptotic methods, the ranges of their applicability are typically not defined exactly, but depend on the magnitude of some parameter. As for rigorous methods, their applicability is limited only by the available computer memory and acceptable computation time, since the integral equations and their approximations remain valid regardless of the frequency and scatterer sizes. Therefore, an agreement between the numerically rigorous and asymptotic solutions attests to the accuracy of both. On the other hand, the limits of applicability of the asymptotics can be refined by the comparison to rigorous numerical solutions validated with the help of the same asymptotics.

In this work, we performed mutual validation of an iterative MLNG-based solver for scalar problems [2] and an asymptotic approximation developed for scattering by strongly elongated spheroids [3, 4].

2 The MLNG-Based Iterative Solver

The MLNG approach and the fast iterative solver on its basis are described in sufficient detail in [2]. Here, we only outline them in brief.

The scatterer is assumed to be a perfectly rigid body immersed in a nonviscous fluid. The scattering problem is formulated in the form of the Burton-Miller hypersingular integral equation [5]. In accordance with the BEM, the scatterer's surface S is triangulated and a basis of N piecewise-constant functions with the supports on the triangles is introduced. Then, after the testing procedure with all N basis functions, the problem formally reduces to a system of N linear algebraic equations, $ZI = V$, where Z is an $N \times N$ matrix.

In the MLNG approach, in order to avoid the $O(N^2)$ storage and $O(N^2)$ computational complexity of calculating the elements of the matrix Z and matrix-vector products ZI when applying iterative methods, the matrix representation of the discretized integral operator is replaced with a less memory-consuming hierarchical tree-like structure. The domain of integration S is divided into progressively smaller subdomains $S_{l,m}$ of progressively lower levels $l = 1$, 2, ..., L, and the parent-child relations between subdomains are established. For each subdomain, except for the top-level ones ($l = 1, 2$), the near and interpolation zones are defined, and to each of them a spherical interpolation grid $\Gamma_{l,m}$ is assigned. For each observation point $\mathbf{r} \in S$, we denote by $S_3(\mathbf{r})$ the union of 3rd-level subdomains to whose near zones the point $\mathbf{r}$ does not belong; by $S_l(\mathbf{r})$, the union of all l-th level subdomains from $S \backslash (S_3(\mathbf{r}) \cup \ldots \cup S_{l-1}(\mathbf{r}))$ to whose near zones $\mathbf{r}$ does not belong; and, by $N(\mathbf{r})$, we denote the complement $S \backslash (S_3(\mathbf{r}) \cup \ldots \cup S_L(\mathbf{r}))$. Thus, for each observation point $\mathbf{r} \in S$, we have a unique decomposition of the domain of integration S into nonintersecting sets:

$$S = N(\mathbf{r}) \cup S_3(\mathbf{r}) \cup \ldots \cup S_l(\mathbf{r}) \cup \ldots \cup S_L(\mathbf{r}). \qquad (1)$$

Since the components of decomposition (1) are nonintersecting, the field produced by sources I on S at the point

$\mathbf{r} \in S$ can be represented by the sum of integrals over these components. The integral over $N(\mathbf{r})$ is calculated directly. The integrals over the other components $S_l(\mathbf{r})$, which consist of selected subdomains $S_{l,m}$, are evaluated by the interpolation to $\mathbf{r}$ of the amplitude-and-phase compensated field stored in the grids $\Gamma_{l,m}$ assigned to them. The result of interpolation is multiplied by the phase-and-amplitude restoration factor, which depends on the point $\mathbf{r}$ and the subdomain $S_{l,m}$. The role of this factor and its reciprocal, the phase-and-amplitude compensation factor, is to compensate the rapidly oscillating e^{-ikr} behavior of the field and improve the accuracy of interpolation (for details, see [2]). This procedure (the MLNG algorithm) enables one to satisfy N testing conditions for a given source field I by asymptotically $O(N \log N)$ rather than $O(N^2)$ operations needed when the same testing conditions are satisfied using matrix Z. The required storage is also on the order of $O(N \log N)$ as opposed to the $O(N^2)$ storage needed for matrix Z. Being applied in combination with the conjugate gradient method, the MLNG algorithm yields an efficient iterative solver.

3 Asymptotic Approximation

Classical short-wave asymptotic expansions in penumbra [6] work perfectly well for cylindrical geometries if the radius is greater than the wavelength λ. Its applicability for spheres requires the radius to be greater than 10–15 λ. For elongated bodies classical asymptotics gives satisfactory results only for bodies longer than several hundred λ. To improve the performance of the asymptotic approximations for the paraxial diffraction by prolate spheroids a new technique have been recently developed [3, 4].

The basic idea of this technique is to fix the relation

$$\frac{ka^2}{p} \equiv \chi = O(1) \qquad (2)$$

between the wavenumber k, the semi-axes: major b and minor a and the half-focal distance $p = \sqrt{b^2 - a^2}$. Then, derivations in the frame of the parabolic equation method written in spheroidal coordinates (ξ, η, ϕ):

$$z = p\xi\eta, \quad r = p\sqrt{\xi^2 - 1}\sqrt{1 - \eta^2},$$

lead to the representation for the forward wave. However, it is slowly attenuated and reaches the shaded tip of the spheroid with a sufficiently large amplitude. In a vicinity of this tip one can approximate the spheroid surface with the surface of the paraboloid and use exact separation of variables in Helmholtz equation rewritten in paraboloidal coordinates. This determines the amplitude of the backward wave. The final representation for the total field on the surface of the hard spheroid can be expressed as

$$u = \frac{4\sqrt{\chi}}{\pi\sqrt{1-\eta^2}} \sum_{n=0}^{+\infty} \frac{i^n \cos(n\phi)}{n!(1+\delta_{n0})} \int_{-\infty}^{+\infty} \left[\frac{1-\eta}{1+\eta}\right]^{it} \Gamma\left(\tfrac{n+1}{2} + it\right) \times$$
$$\times \frac{M_{it,n/2}(i\beta^2)}{\beta} \frac{e^{ikp\eta} + r_n(t) e^{-ikp\eta}}{iW_{it,n/2}(-i\chi) - 2\chi W'_{it,n/2}(-i\chi)} dt. \qquad (3)$$

Here δ_{n0} is the Kronecker delta, while M and W are the Whittaker functions. The angle of incidence θ is present in (3) via parameter $\beta = \sqrt{kp}\theta$, which is assumed to be bounded when $kp \to \infty$. The second term in the numerator of the last fraction in (3) corresponds to the backward wave and

$$r_n = (-i)^{n+1} e^{2ikp} (4kp)^{-2it} \frac{\Gamma\left(\frac{n+1}{2} + it\right)}{\Gamma\left(\frac{n+1}{2} - it\right)}.$$

When kp is very large, r_n rapidly oscillate with respect to t and the backward wave contribution can be neglected.

Usually it is sufficient to sum up no more than 10 angular harmonics in (3) and the essential part of the integration domain is usually bounded by $|t| < 10$. However, the specifics of the asymptotic approximation (3) is in the requirement that parameters χ and β remain bounded. The increase of β may result in the necessity to take into account more angular harmonics and it also extends the domain of integration towards positive values of t. Larger values of χ require the integration interval to be extended in the negative direction.

4 Comparison

The applicability of the asymptotic approximation (3) imposes some restrictions on the parameters of the test problems. Namely, the spheroid should be sufficiently elongated (parameter χ should not be large) and the angle of incidence should be small (parameter β should not be large). For the numerical experiments we use two hard spheroids, both having the length of 10 m, but different aspect ratios 1:5 (spheroid A) and 1:10 (spheroid B). We compare the values of the acoustic pressure fields on the surface excited by a plane wave at different frequencies and angles of incidence. In the case of axial incidence, the amplitudes of the fields are compared in Fig. 1 for spheroid A and Fig. 2 for spheroid B. For low frequencies, the difference between

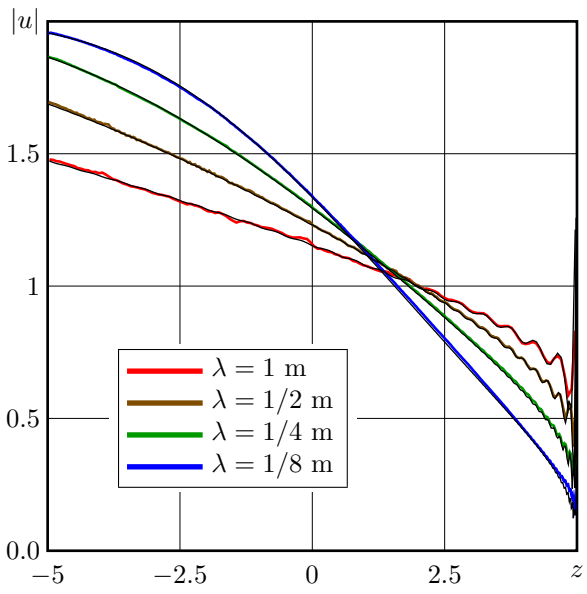

Figure 1. Amplitudes of the field on spheroid A.

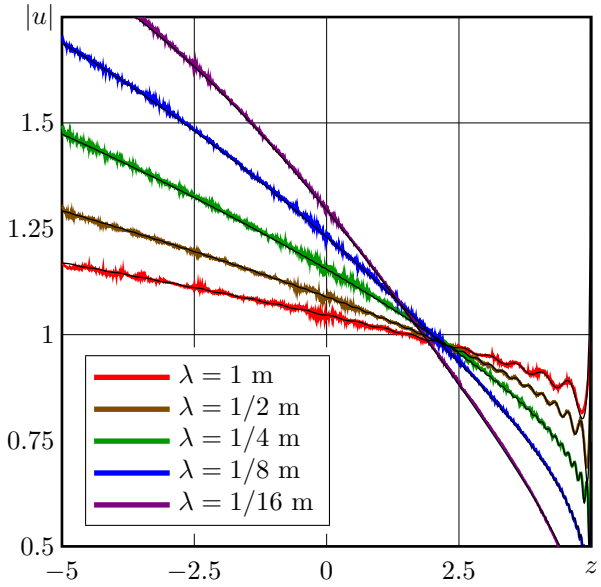

Figure 2. Amplitudes of the field on spheroid B.

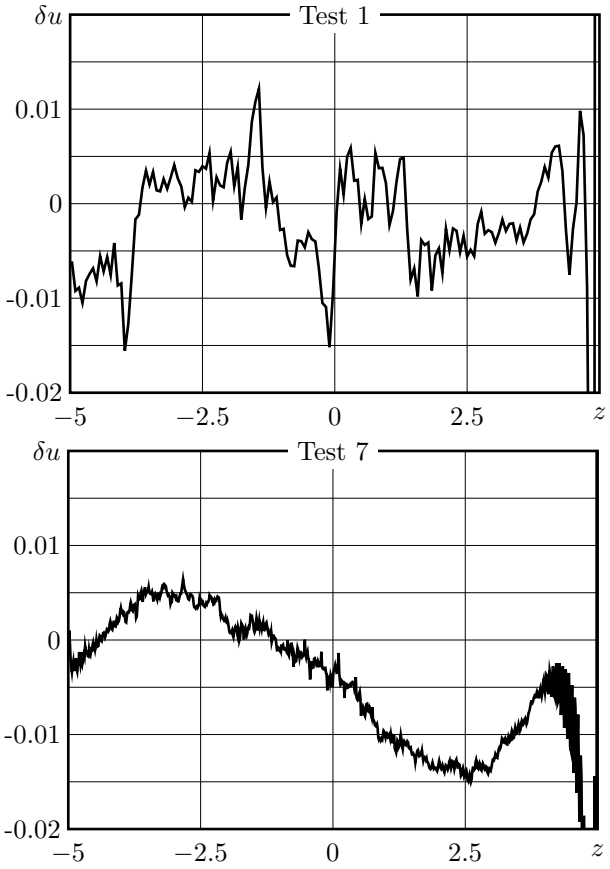

Figure 3. The difference (asymptotic minus numeric) of results for axial incidence on spheroid A with $\lambda = 1$ m (Test 1) and $\lambda = 1/8$ m (Test 7).

the asymptotic and numerical results have random character, but when the frequency increases one can notice some systematic error, see Fig. 3. For more elongated spheroids, the systematic error is not observed even at two times higher

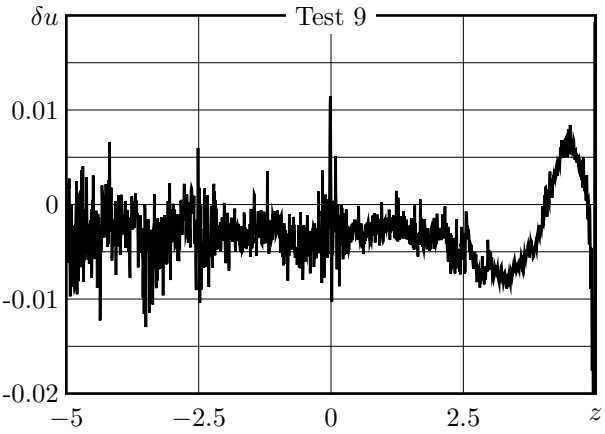

Figure 4. The difference (asymptotic minus numeric) of results for axial incidence on spheroid B with $\lambda = 1/16$ m.

frequency, see Fig. 4. Therefore this systematic error can be due to the error of the asymptotic approximation. However, such error is not present in the electromagnetic variant of the asymptotic approximation as have been checked in [7].

The fast solver computes the fields at the centroids of the mesh. So, to get the cuts presented on Figs. 1–4 some additional computations are needed. However, it is possible to compute asymptotic approximations exactly at the same points on the surface and then calculate the norms of the differences. We compare both the amplitudes of the fields $\delta_1 = |u_a| - |u_f|$ and the complex values $\delta_2 = u_a - u_f$, where u_a is the result obtained with the use of the asymptotic approximation (3) and u_f is the value computed by the fast solver. The differences δ_2 includes highly oscillatory factor and therefore are more sensitive to the parameter kp. Table 1 presents the ℓ_1 norms of the errors. In

Table 1. The ℓ_1 norms of the errors for $\lambda = 2^{(1-n)/2}$ m.

n	centroids	$\theta = 0^\circ$		$\theta = 10^\circ$	
Spheroid A		$\|\delta_1\|$	$\|\delta_2\|$	$\|\delta_1\|$	$\|\delta_2\|$
1	11232	0.0072	0.0192	0.0077	0.0207
2	21624	0.0078	0.0217	0.0082	0.0235
3	42076	0.0082	0.0231	0.0083	0.0255
4	85816	0.0081	0.0268	0.0082	0.0299
5	169344	0.0085	0.0283	0.0087	0.0329
6	328852	0.0075	0.0433	0.0084	0.0361
7	644252	0.0087	0.0419	0.0085	0.0420
8	1261324	0.0088	0.0720	0.0079	0.0327
Spheroid B		$\|\delta_1\|$	$\|\delta_2\|$	$\|\delta_1\|$	$\|\delta_2\|$
1	10486	0.0019	0.0049	0.0028	0.0064
2	10486	0.0036	0.0074	0.0036	0.0076
3	44180	0.0017	0.0040	0.0021	0.0063
4	44180	0.0032	0.0060	0.0029	0.0063
5	88124	0.0038	0.0074	0.0038	0.0123
6	174530	0.0039	0.0077	0.0037	0.0085
7	355243	0.0041	0.0088	0.0051	0.0204
8	714224	0.0039	0.0090	0.0044	0.0106
9	1476190	0.0048	0.0111	0.0059	0.0362

order to obtain correct asymptotic approximation for the field on Spheroid A at the highest numerically accessible frequency ($\lambda = 2^{-7/2}$ m) for the incidence at 10°, the number of modes, which have been taken into account has been increased to 20. For all the other cases it was set equal to 10.

5 Conclusions

The comparison has shown that the difference between the surface fields calculated using the MLNG-based solver and the asymptotic approximation is generally within 1% in the integral norm if only the absolute values are compared and about twice as large if the phases are also taken into account. Most of this deviation is due to the numerical noise caused by the use of zero-order basis functions in the MLNG-based solver, which proved to be about 1%. This fairly good agreement demonstrates the accuracy of both methods and, in particular, provides a nontrivial validation for the MLNG-based solver, which in turn supports its application to a much wider class of scatterers.

References

[1] J. M. Song and W. C. Chew, "Multilevel fast-multipole algorithm for solving combined-field integral equations of electromagnetic scattering", *Microw. Opt. Technol. Lett.*, **10**, September 1995, pp. 14–19.

[2] E. Chernokozhin, Y. Brick, and A. Boag, "A fast and stable solver for acoustic scattering problems based on the nonuniform grid approach", *J. Acoust. Soc. Am.*, **139**, 1, January 2016, pp. 472–480.

[3] I. V. Andronov, "Diffraction by a strongly elongated body of revolution", *Acoustical Physics*, **57**, 2, 2011, pp. 121–126.

[4] I. V. Andronov, "High-frequency acoustic scattering from prolate spheroids with high aspect ratio", *J. Acoust. Soc. Am.*, **134**, 6, 2013, pp. 4307–4316.

[5] A. J. Burton and G. F. Miller, "The application of integral equation methods to the numerical solution of some exterior boundary-value problems", *Proc. R. Soc. London, Ser A*, **323**, 1971, pp. 201–210.

[6] V. A. Fock, *Electromagnetic Diffraction and Propagation Problems*, Pergamon Press, 1965.

[7] I. V. Andronov, D. Bouche, and M. Duruflé, "High-frequency currents on a strongly elongated spheroid", *IEEE Trans. Antennas Propag.*, **65**, 2, 2017, pp. 794–804.